# Lidar observations of neutral Fe layers and fast gravity waves in the thermosphere (110–155 km) at McMurdo (77.8°S, 166.7°E), Antarctica

Xinzhao Chu,[1] Zhibin Yu,[1] Chester S. Gardner,[2] Cao Chen,[1] and Weichun Fong[1]

Received 13 October 2011; revised 5 November 2011; accepted 7 November 2011; published 15 December 2011.

[1] We report the first lidar observations of neutral Fe layers with gravity wave signatures in the thermosphere from 110–155 km at McMurdo, Antarctica in May 2011. The thermospheric Fe densities are low, ranging from ∼200 $cm^{-3}$ at 120 km to ∼20 $cm^{-3}$ at 150 km. The measured temperatures from 115–135 km are considerably warmer than MSIS and appear to be related to Joule heating enhanced by aurora. The observed waves originate in the lower atmosphere and show periods of 1.5–2 h through 77–155 km. The vertical wavelength increases from ∼13 km at 115 km to ∼70 km at 150 km altitude. These wave characteristics are strikingly similar to the traveling ionospheric disturbances caused by internal gravity waves. The thermospheric Fe layers are likely formed through the neutralization of vertically converged $Fe^+$ layers that descend in height following the gravity wave downward phase progression. **Citation:** Chu, X., Z. Yu, C. S. Gardner, C. Chen, and W. Fong (2011), Lidar observations of neutral Fe layers and fast gravity waves in the thermosphere (110–155 km) at McMurdo (77.8°S, 166.7°E), Antarctica, *Geophys. Res. Lett.*, *38*, L23807, doi:10.1029/2011GL050016.

## 1. Introduction

[2] Thermospheric gravity waves with periods of 1–2 h have been observed as traveling ionospheric disturbances (TIDs) in electron density between 120 and 400 km [e.g., *Djuth et al.*, 2010, and references therein]. These waves exhibit downward phase progression and their phase speeds and vertical wavelengths increase substantially with increasing altitudes. However, such waves have never been observed in the neutral metallic atoms in the thermosphere above 110 km, because the meteoric metal layers such as Fe, Na and K are normally confined to altitudes of 75–115 km [*Plane*, 2003]. Although the 'topside layer' has been reported up to 130 km [*Höffner and Friedman*, 2005], and sporadic Fe, Na and K layers have been observed above 100 km [e.g., *Kane et al.*, 1993], lidar observations have shown neither the neutral layers above 130 km nor the gravity waves above 110 km. Consequently, the studies of dynamics and thermal structure by lidars have been limited to the lower thermosphere.

[3] In this paper we report the first (to our knowledge) observations of thermospheric gravity waves in the neutral Fe layers from 110 to 155 km, made with an Fe Boltzmann temperature lidar on 2 and 28 May 2011 at McMurdo (77.83°S, 166.66°E), Antarctica. As a southern polar site, McMurdo is located at high geographic and magnetic latitudes, and is near the poleward edge of the aurora oval. The low solar background during long dark polar nights facilitates the detection of weak metallic layers in the thermosphere. The unique geomagnetic conditions at McMurdo may also provide opportunities to study how the neutral and ionized Fe layers are connected in the E-region and how the thermosphere is affected by Joule heating. It is now known that Fe atoms are the most abundant metal species in the Earth's upper atmosphere, while $Fe^+$ ions are a major component of sporadic E layers [*Plane*, 2003]. Photo ionization and charge transfer are usually strong above 110 km, which facilities the production of $Fe^+$ and loss of Fe. As a result, the existence of neutral Fe layers up to 155 km poses interesting questions of how the neutral Fe atoms are formed in the thermosphere and how gravity waves produce signatures in the Fe layers. Several hypotheses will be discussed following our report of the observations.

## 2. Observations

[4] The University of Colorado lidar group installed the Fe Boltzmann lidar at Arrival Heights, McMurdo in Dec 2010, with support from the United States Antarctic Program and Antarctic New Zealand [*Chu et al.*, 2011]. This lidar consists of two independent channels probing respectively the 372 and 374 nm absorption lines of neutral Fe atoms. By employing the Fe Boltzmann technique, temperatures can be inferred from the signal ratios between these two channels. Principles, capabilities and error analysis of the lidar are described by *Chu et al.* [2002].

[5] Illustrated in Figures 1a and 1b are the normalized photon counts of neutral Fe layers from 70 to 155 km measured by the 372- and 374-nm lidar channels, respectively, on 28 May 2011. In both plots, the main layers are distributed from ∼75 to 110 km with sharp bottom edges but slower decay on the topside, which is consistent with observations of Fe layers elsewhere [e.g., *Plane*, 2003]. However, the distinct Fe layers above 110 km with apparent wave features are unique and have never been reported before. The thermospheric Fe is clear at the beginning of the observation (11.5 UT) with a distinguishable layer up to 133 km. The layer descends with time and merges with the main layer at ∼110 km around 13.5 UT. In the meantime, another Fe layer develops at ∼145 km and then descends downward. The third and highest Fe layer occurs around 14.7 UT at 155 km

[1]Cooperative Institute for Research in Environmental Sciences and Department of Aerospace Engineering Sciences, University of Colorado at Boulder, Boulder, Colorado, USA.
[2]Department of Electrical and Computer Engineering, University of Illinois at Urbana-Champaign, Urbana, Illinois, USA.


0094-8276/11/2011GL050016

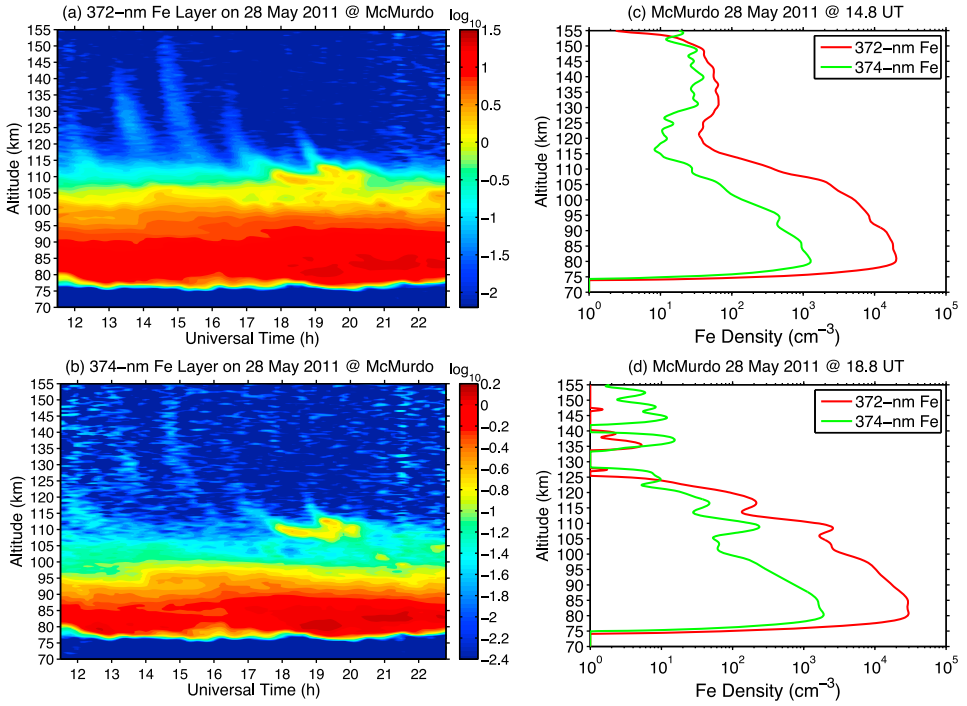


**Figure 1.** Observations of neutral Fe layers by the 372- and 374-nm lidar channels on 28 May 2011 (UT) at McMurdo, Antarctica. (left) Plotted in $\log_{10}$ scale are contours of Fe photon counts normalized to the Rayleigh signals at 45 km for the (a) 372-nm and (b) 374-nm channels. (right) The vertical profiles of Fe densities derived for (c) 14.8 UT and for (d) 18.8 UT. The raw data with resolutions of 1 min and 48 m are smoothed with Hamming windows of 0.25 h and 0.5 km for Figures 1a and 1b and 0.25 h and 2 km for Figures 1c and 1d (FWHM). The uncertainty of 372-nm Fe density in Figure 1c is 20–30% above 120 km and much less below 110 km.

and then descends with time. The wave-like features repeat four more times before the termination of the observations due to clouds, but the starting altitudes of the Fe layers become lower as time progresses. The 6th and 7th layers starting below 120 km are barely visible. Interestingly, when the 4th and 5th layers descend below 115 km, two distinct sporadic Fe layers occur in the range of 105–115 km between 18 and 20.5 UT, standing out clearly in both Fe contours. The striking similarities between these two independent channels and the clear wave signatures make the lidar detection of thermospheric Fe layers unequivocal.

[6] To further quantify the thermospheric Fe layers, we compute Fe temperatures from two channels of normalized photon counts using the Boltzmann technique, and convert the 372-nm counts to Fe densities [*Chu et al.*, 2002]. In the density derivation, the lidar effective cross sections are calculated using the derived Fe temperatures in the MLT region and MSIS-00 temperatures above 110 km. Two representative vertical profiles of Fe densities are plotted in Figures 1c and 1d. The profiles of the highest Fe layer at 14.8 UT exhibit appreciable Fe densities above 115 km in both 372 and 374 nm channels, when compared to the profiles for 18.8 UT. The noise levels above 130 km in Figure 1d, where the Fe layer disappears, establish detection limits for both channels of $\sim$3 cm$^{-3}$. The number densities in the 372-nm Fe layer vary from $\sim$65 cm$^{-3}$ at 130 km to $\sim$20 cm$^{-3}$ at 150 km, as inferred from Figure 1c, which are small when compared to the main layer peak density of $\sim$20,000 cm$^{-3}$. The 374-nm densities are about 2–4 times lower than the 372-nm densities from 120 to 150 km, but well above the background noise.

[7] A contour of thermospheric Fe density is illustrated in Figure 2a. The wave signatures in the Fe layers are very clear. The peak densities vary, with a maximum close to 110 cm$^{-3}$ around 125 km at 13.5 UT. In between two distinct crests the Fe densities vary from $\sim$10 cm$^{-3}$ at 130 km to $\sim$3 cm$^{-3}$ at 150 km. Consequently, the ratios of the Fe densities between crests and troughs are about 4–15 in this altitude range. Such wave-induced Fe density perturbations are much larger than the concomitant perturbations in the neutral atmosphere and the electron density [e.g., *Djuth et al.*, 2010]. Fe temperatures plotted in Figure 2b for the main Fe layers show apparent wave perturbations throughout the observations. The dominant wave has a period of $\sim$8 h and vertical phase velocity of $-$0.7 m/s. Shorter-period waves of $\sim$1.5 h are clearly visible below 90 km. The mesopause is located near 100 km with a temperature of $\sim$190 K. Taking the highest Fe layer that goes to 155 km, we derive the Fe temperatures from 75 to 150 km using the Boltzmann technique. Combining with the Rayleigh integration technique, the Fe lidar is able to measure temperatures from 30 to 150 km as shown in Figure 2c. Also plotted are the MSISE-00 temperatures for McMurdo location on 28 May 2011. The MSIS temperatures are close to the lidar data below 110 km. Above 115 km and below 135 km, the Fe temperatures are much warmer than MSIS, and the difference is up to $\sim$600 K at 132 km.

[8] Both lidar channels show the same wave features in the thermosphere from 110 to 155 km. The wave has a downward phase progression. The vertical phase speed is the largest at the highest altitude but around 125 km the phase speed decreases quickly with decreasing altitude. The

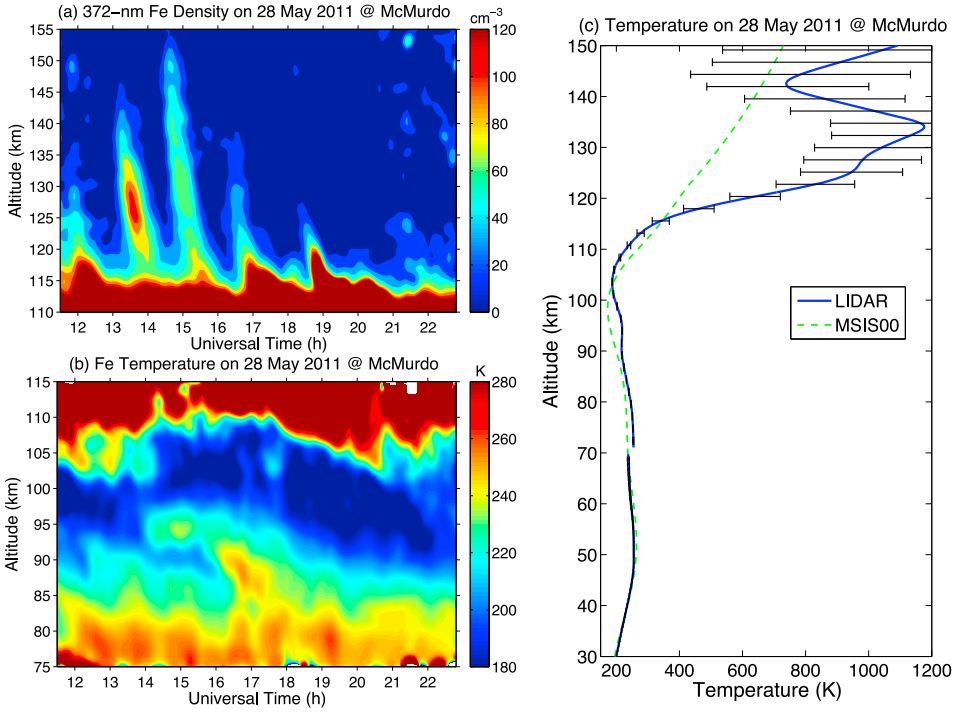


**Figure 2.** Event on 28 May 2011 at McMurdo, Antarctica: (a) contour of thermospheric Fe densities from 110 to 155 km, showing fast gravity waves in the thermosphere, (b) contour of Fe temperatures from 75 to 115 km, showing waves in the MLT region, and (c) the vertical profile of temperatures for 1 h integration around 15 UT. The temperature errors plotted as horizontal bars in Figure 2c are less than 5 K below 110 km. Rayleigh lidar temperatures are plotted below 70 km.

vertical wavelength is shortest at 115 km and increases significantly with increasing altitude. Spectral analysis of the Fe layers using wavelet shows that the period $T$ of the wave (~1.5 h) is nearly constant through the 115–155 km range (Figure 3a). By tracking the peak Fe contour, we obtain the phase line (altitude vs. time) in the thermosphere, and then the vertical phase speeds $c_z$ are derived by taking the derivative of the phase line altitude with respect to time. The vertical wavelengths $\lambda_z$ are then calculated as $\lambda_z = c_z \cdot T$. As shown in Figure 3b, the downward phase speed increases from ~2 m/s at 115 km to over 10 m/s above 135 km. The vertical wavelength $\lambda_z$ varies from ~13 km at 115 km to ~70 km around 150 km. These wave characteristics, especially the changes of $c_z$ and $\lambda_z$ with height, closely resemble the thermospheric gravity waves observed as TIDs in the electron density perturbations by incoherent scatter radar (ISR) [e.g., *Djuth et al.*, 2010]. The wave period of ~90 min in the Fe layer is longer than the TIDs observed at Arecibo Observatory by *Djuth et al.* [2010], but TIDs can have periods from 20 min to several hours according to *Thome* [1964]. The downward phase progression indicates the upward propagation of the wave energy. The wave likely originated from the atmosphere below 75 km [*Vadas and Nicolls*, 2009], not from an aurora source above 150 km [*Richmond*, 1978]. In the MLT region, the Fe temperature contour (Figure 2b) exhibits short-period waves in addition to the dominant 8-h wave. In order to extract such wave information, we derive the relative temperature perturbations from Figure 2b. After subtracting the dominant 8-h wave, a wavelet analysis reveals the wave period around 1.5 h with errors less than 0.3 h from 75 to 115 km, as plotted in Figure 3a. The corresponding $c_z$ and $\lambda_z$ are plotted in Figure 3b. Note that the observed wave period can change in time if the background wind changes rapidly [*Eckermann and Marks*, 1996]. The waves in the MLT region are in general consistent with the thermospheric gravity waves, supporting the hypothesis that the waves originated from the lower atmosphere below 75 km.

[9] A similar thermospheric wave event was also observed on 2 May 2011 at McMurdo. As illustrated in Figure 4a, signatures of neutral Fe layers occur in the thermosphere three times around 9.7, 11.8 and 14 UT, with a wave period of slightly over 2 h. The strongest layer occurs around

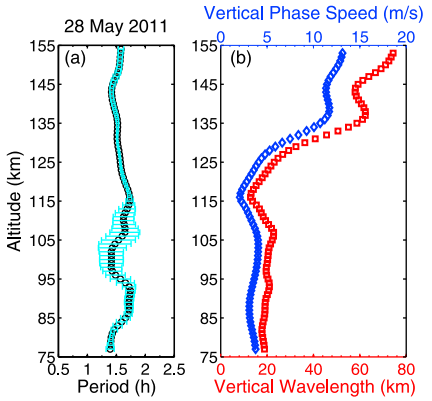


**Figure 3.** Ground-based (a) gravity wave period along with (b) vertical phase speed (blue diamonds) and vertical wavelength (red squares) derived for the event on 28 May 2011 at McMurdo. The period errors are plotted as horizontal bars in Figure 3a.

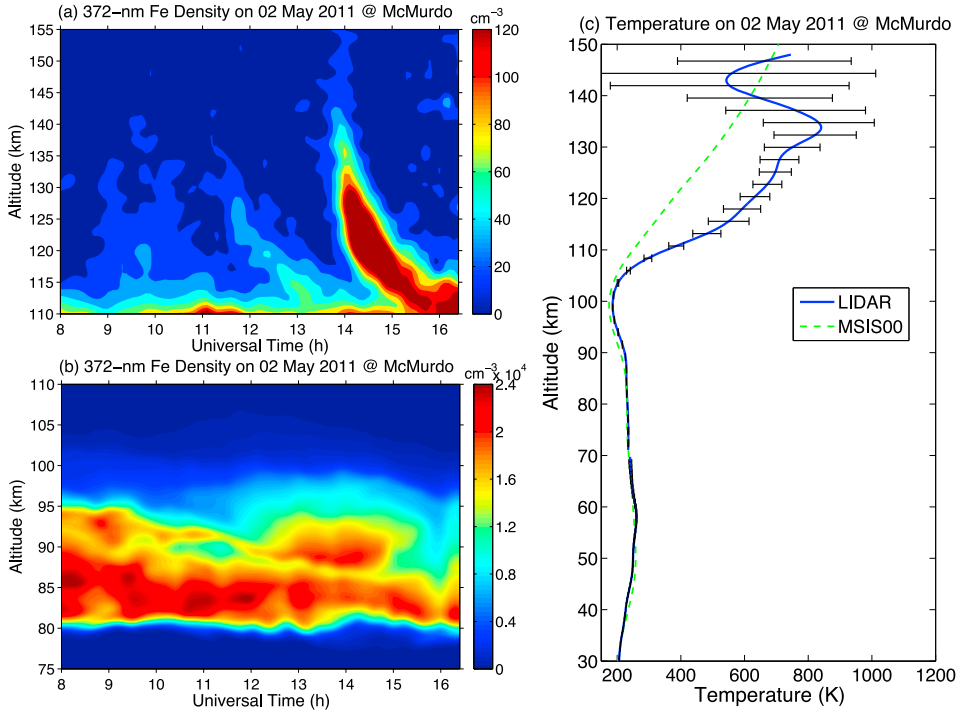


**Figure 4.** Event on 2 May 2011 at McMurdo, Antarctica: (a) the 372-nm Fe density contour in the thermosphere, (b) the 372-nm Fe density in the MLT, and (c) the lidar temperature profile for 1-h integration around 14 UT. The temperature errors (horizontal bars) are less than 5 K below 105 km. Rayleigh lidar temperatures are plotted below 70 km.

14 UT, reaching the highest altitude of ~155 km and with the maximum Fe density of ~200 cm$^{-3}$ at 120 km. The shape of the layers is similar to the event on 28 May 2011. Figure 4b shows the main Fe layers in the MLT. The Fe Boltzmann temperatures within the strongest layer were derived from 75 to 150 km in Figure 4c. Also plotted are the Rayleigh lidar temperatures and the MSIS-00 temperatures at McMurdo for 2 May 2011. The lidar and MSIS-00 temperatures agree well below 105 km. Above 105 km and below 135 km, the Fe temperatures are significantly warmer than the MSIS, similar to the situation on 28 May 2011. The similarities between these two events observed on two different days further confirm the robustness of the lidar detection of neutral Fe layers, elevated temperatures and gravity waves in the thermosphere. Among the 233 h of lidar observations made on 14 days from May through August 2011, thermospheric Fe layer events above 120 km occurred on at least 5 other days. These events were observed for at least 41 h, giving an occurrence frequency of ~18%.

## 3. Discussion

[10] We believe that this is the first report of neutral Fe layers up to 155 km and also the first observations of gravity waves in metal layers at such high altitudes. How the neutral Fe layers are formed in the E region and how they exhibit such wave signatures are challenging questions. It is unlikely that these neutral atoms are ejected or diffused directly from the main Fe layers in the MLT region, because the expected shape in the time-altitude domain would extend upward from, rather than descend towards, the main layer. The second possible source of neutral Fe is the direct meteor ablation or sputtering off smoke particles. *Plane* [2003] points out that the ablation altitude depends on the entry velocity of meteoroids, and even very fast meteoroids of 40 km/s ablate below 125 km with peak ablation at 101 km, while slow meteoroids peak at 92 km. Furthermore, the differential ablation process releases the volatile constituents (Na and K) first. Fe and Mg are released from the molten meteoroid only after the temperature exceeds ~1800 K. As a result, Fe has peak injection rates around 85 km, with Na and K ~8 km higher [*Vondrak et al.*, 2008; *Janches et al.*, 2009]. Such a height profile of ablation cannot explain the observations. If we assume sputtering exists above 110 km or molecular diffusion somehow distributes neutral Fe to 155 km, waves are unlikely to cause sufficient perturbations of the neutral atmosphere to account for the observed "high contrast" of the Fe layers.

[11] Most likely the observed thermospheric Fe layers are linked to the layered $Fe^+$ ions that are then neutralized to produce neutral Fe atoms. First, the shape of the observed layers in Figures 2a and 4a indicates descending layers from higher to lower altitude as time progresses, similar to the motions of ion layers observed by the ISR [*Mathews et al.*, 1993]. Secondly, the ratio of the wave crest and trough being far larger than any perturbations in the neutral atmosphere suggests that the Fe layers are related to ions that have been layered by various forces in the thermosphere [*Carter and Forbes*, 1999]. Thirdly, the changes of vertical wavelengths and phase speeds are similar to the TIDs [e.g., *Djuth et al.*, 2010] and are consistent with theoretical expectations for gravity waves [*Vadas*, 2007; *Vadas and Nicolls*, 2009].

[12] The hypothesis of layered $Fe^+$ being converted to neutral Fe faces several critical issues: the sources of $Fe^+$, the formation of $Fe^+$ layer and its shape, neutralization

mechanisms to convert $Fe^+$ to Fe, and transport of Fe and $Fe^+$. Aurora heating in the polar cap may cause upwelling and thus upward transport of $Fe^+$ or Fe into the thermosphere [*Burns et al.*, 1991]; however, this mechanism is unproven at these low altitudes. *Carter and Forbes* [1999] point out that the redistribution of meteor deposited $Fe^+$ in the meridional plane by electric fields is most pronounced at low latitudes in connection with the "fountain effect". Gravity and diffusion redistribute $Fe^+$ along field lines, and $Fe^+$ can reach the F region. Although the fountain effect may not be effective in the Polar Regions, $Mg^+$ ions have been observed by satellites in the thermosphere up to 300 km in the polar region [*Viereck et al.*, 1996]. Considering Fe and Mg have similar ablation altitudes [*Vondrak et al.*, 2008], it is reasonable to assume that $Fe^+$ ions are distributed in the E and F regions over McMurdo. The formation of $Fe^+$ layers at McMurdo should share the same mechanisms as the TIDs and sporadic E layers at high latitudes. The observed shape indicates that vertically converged ion layers descend in height with time, following the gravity wave downward phase progression. The wave-induced wind shears in combination with the geomagnetic and electric fields provide the needed vertical convergence of ions [e.g., *Hines*, 1963; *Kelley*, 1989; *Bristow and Watkins*, 1991; *Carter and Forbes*, 1999; *Djuth et al.*, 2010]. Layers formed by electrical fields have no systematic vertical motion, unlike the layers produced by gravity-wave wind shears. Wind shears descend with the downward phase velocities of the wave, resulting in the downward transport of the layers. The simultaneous occurrence of two layers at the bottom and top of the profiles in Figures 2a and 4a, and the repeated layer shapes, supports the wave phase idea. Because the shorter vertical wavelength, slower phase speed waves dominate the power spectral density in the MLT region but dissipate rapidly when propagating upward [*Vadas*, 2007], the longer wavelength and faster vertical phase speed waves show up more clearly at higher altitudes as we observed. The increase of $\lambda_z$ with altitude above 115 km is likely due to a decrease of $N^2$ (buoyancy frequency) and an increase of the neutral wind component in an opposite direction to the wave propagation [*Vadas and Nicolls*, 2009].

[13] Conversion from $Fe^+$ ions to neutral Fe in the thermosphere is likely through the direct electron recombination: $Fe^+ + e^- \rightarrow Fe + h\nu$, as $Fe^+$ is neutralized essentially only by radiative recombination with electrons at altitudes above ~120 km [*Plane et al.*, 2003; *Zhou et al.*, 2008]. Although the value of the reaction rate coefficient is small and given as $4 \times 10^{-12}$ cm$^3$ s$^{-1}$ to $1 \times 10^{-11}$ cm$^3$ s$^{-1}$ by *Plane* [2003] and *Plane et al.* [2003], it is large enough to produce the Fe densities observed. This is because the Fe density (20–100 cm$^{-3}$) is a small fraction of the $Fe^+$ density in sporadic E layers, and the loss rate of neutral Fe in the dark polar night is small. Note that 12.89 UT is the local midnight at McMurdo. The lidar observations reported here span 8–24 UT, corresponding to the local time from 19–11 LT. The solar declination angles on 2–28 May 2011 were 15.6°–21.6°, giving total darkness below 155 km when the thermospheric Fe layers were observed, so photo-ionization of Fe neutrals is absent. The recombination of $O_2^+$ and $NO^+$ with electrons proceeds fast with a rate coefficient of ~$3 \times 10^{-7}$ cm$^3$ s$^{-1}$, leading to 30 s to ~1 h lifetime of $O_2^+$ and $NO^+$ depending on electron density. Therefore, these ion densities decay rapidly in the polar night. Assuming their total density is less than $1 \times 10^4$ cm$^{-3}$ and the reaction rate coefficient of charge transfer between Fe and $O_2^+$ / $NO^+$ is ~$1 \times 10^{-9}$ cm$^3$ s$^{-1}$ [*Plane et al.*, 2003], the neutral Fe loss rate by charge transfer is estimated as $k([O_2^+] + [NO^+]) = 10^{-5}$ s$^{-1}$. This gives an Fe lifetime of ~27 h during dark night, much longer than the wave period but comparable to the Fe lifetime of 33 h estimated by *Zhou et al.* [2008]. On the other hand, the production rate for converting $Fe^+$ to Fe is given by $k[Fe^+]N_e$, where $N_e$ is the electron number density. Assuming $N_e$ in the sporadic E layer is $1 \times 10^5$ cm$^{-3}$ and $[Fe^+]$ occupies most of the ion density, the Fe production rate ranges from $4 \times 10^{-2}$ cm$^{-3}$ s$^{-1}$ to $1 \times 10^{-1}$ cm$^{-3}$ s$^{-1}$. Therefore, neutral Fe densities of 40–100 cm$^{-3}$, comparable to observations, can be produced within 1000 s, much shorter than the wave period (~5,500 s). The transport of converted Fe is likely different than that of $Fe^+$. While the wave transports $Fe^+$ downward, the wave motion may not affect the neutral Fe atoms that are left in the wake of $Fe^+$ layers. This leads to slight height difference with the Fe layer located above the $Fe^+$ layer, as observed in sporadic Na and E layers above 100 km by *Kane et al.* [1993].

[14] Strong aurora was observed at McMurdo on 28 May 2011, corresponding to a geomagnetic storm with the Kp index increased to 6 after 6 UT and lasted until 15 UT. In the case on 2 May 2011, the geomagnetic conditions were relatively quiet but weak aurora was visually seen over McMurdo during the lidar measurements. Auroral particle precipitation may have several effects on the events. They may increase the electron density to facilitate the conversion from $Fe^+$ to Fe; but it may also shorten the lifetime of Fe by direct ionization and by increasing the density of $O_2^+$ and $NO^+$ to accelerate charge transfer. The electric fields associated with aurora will increase the Joule heating of neutral atmosphere and frictional heating of ions. Though frictional heating can heat up ions to over 1000 K [*Maeda et al.*, 2005], what we measured directly is neutral Fe. The freshly converted Fe can have elevated temperatures above the background. Thermalization via collisions with surrounding neutrals only takes about 1–2 s even at 150 km where the collision rate is ~20 s$^{-1}$. However, the above analysis suggest that the neutral Fe atoms have a lifetime on the order of 1000 s; therefore, majority of observed Fe atoms are likely in thermodynamic equilibrium with the surroundings. The mixture of freshly converted and thermalized Fe likely results in Fe temperatures closer to the background neutrals, rather than the ions. Joule heating rates measured by ISR range from $0.1 \times 10^{-6}$ to $1 \times 10^{-6}$ W/m$^3$, and the neutral gas heating rates are 0.02–0.08 K/s from 110 to 135 km [*Thayer and Semeter*, 2004, and references therein]. If the aurora-enhanced heating has been going on for several hours before the lidar observations started, a significant temperature increase in the neutrals can occur, as observed. The observation of warmer temperatures on May 28 compared to May 2 is consistent with the geomagnetic activities at McMurdo.

## 4. Conclusions

[15] Neutral Fe layers with gravity wave signatures were observed for the first time in the thermosphere from 110 to 155 km by both the 372- and 374-nm channels of an Fe Boltzmann temperature lidar at McMurdo, Antarctica on 2 and 28 May 2011. The Fe densities are quite low

(20–200 $cm^{-3}$) in the altitude range of 120–150 km, but sufficient for temperature derivation. Combining the Fe Boltzmann and Rayleigh integration techniques, we are able to derive temperatures from 30 to 150 km using the Fe lidar. While comparable to the MSIS data below 110 km, the lidar temperatures are significantly warmer than MSIS between 115 and 135 km during both events. These elevated temperatures appear to be related to the Joule heating enhanced by aurora. The observed waves originate from the lower atmosphere and show nearly constant periods of 1.5–2 h through the range of 75–155 km. The downward phase speeds are large at high altitudes, decrease with decreasing altitude and are curved towards increasing time. The vertical wavelengths vary from 13 km at 115 km to ~70 km at 150 km. These wave characteristics closely resemble the TIDs and are consistent with the theoretical expectations for gravity waves. The observed thermospheric Fe layers are most likely linked to the layered $Fe^+$ ions that are neutralized to produce Fe. Vertically converged $Fe^+$ ion layers descend in height with time, following the gravity wave downward phase progression, which forms the observed layer shape. It is likely that the direct recombination with electron converts $Fe^+$ to Fe during the dark polar night. Geomagnetic activities like aurora may have played roles in the observed events. Quantitative explanations of these events require detailed modeling studies of $Fe^+$ source and layering, Fe formation and loss, gravity wave source and propagation, and the transport of $Fe^+$ and Fe at high latitudes, along with simultaneous measurements of Fe, $Fe^+$ and electrons. Certainly, the observations of neutral Fe layers, elevated neutral temperatures and gravity waves in the thermosphere over McMurdo challenge our understanding of upper atmosphere chemistry, composition, dynamics and thermal structure.

[16] **Acknowledgments.** We sincerely acknowledge Wentao Huang, Zhangjun Wang and John A. Smith for their contributions to the lidar campaign. We are very grateful to Art Richmond, Jeff Forbes, Jeff Thayer, John Plane, Rich Collins, Alan Burns, Jonathan Friedman and Vladimir Papitashvili for valuable discussions. We thank the staff of United States Antarctic Program, McMurdo Station, Antarctic New Zealand and Scott Base for their support. This project was supported by the National Science Foundation (NSF) grant ANT-0839091.

[17] The Editor thanks Jia Yue and an anonymous reviewer for their assistance in evaluating this paper.

## References

Bristow, W. A., and B. J. Watkins (1991), Numerical simulation of the formation of thin ionization layers at high latitudes, *Geophys. Res. Lett.*, *18*, 404–407, doi:10.1029/90GL02588.

Burns, A. G., T. L. Killeen, and R. G. Roble (1991), A theoretical study of thermospheric composition perturbations during an impulsive geomagnetic storm, *J. Geophys. Res.*, *96*, 14,153–14,167, doi:10.1029/91JA00678.

Carter, L. N., and J. M. Forbes (1999), Global transport and localized layering of metallic ions in the upper atmosphere, *Ann. Geophys.*, *17*, 190–209, doi:10.1007/s00585-999-0190-6.

Chu, X., et al. (2002), Fe Boltzmann temperature lidar: Design, error analysis, and first results from the north and south poles, *Appl. Opt.*, *41*, 4400–4410, doi:10.1364/AO.41.004400.

Chu, X., W. Huang, W. Fong, Z. Yu, Z. Wang, J. A. Smith, and C. S. Gardner (2011), First lidar observations of polar mesospheric clouds and Fe temperatures at McMurdo (77.8°S, 166.7°E), Antarctica, *Geophys. Res. Lett.*, *38*, L16810, doi:10.1029/2011GL048373.

Djuth, F. T., L. D. Zhang, D. J. Livneh, I. Seker, S. M. Smith, M. P. Sulzer, J. D. Mathews, and R. L. Walterscheid (2010), Arecibo's thermospheric gravity waves and the case for an ocean source, *J. Geophys. Res.*, *115*, A08305, doi:10.1029/2009JA014799.

Eckermann, S. D., and C. J. Marks (1996), An idealized ray model of gravity wave-tidal interactions, *J. Geophys. Res.*, *101*, 21,195–21,212, doi:10.1029/96JD01660.

Hines, C. O. (1963), The upper atmosphere in motion, *Q. J. R. Meteorol. Soc.*, *89*, 1–42, doi:10.1002/qj.49708937902.

Höffner, J., and J. S. Friedman (2005), The mesospheric metal layer topside: Examples of simultaneous metal observations, *J. Atmos. Sol. Terr. Phys.*, *67*, 1226–1237, doi:10.1016/j.jastp.2005.06.010.

Janches, D., L. P. Dyrud, S. L. Broadley, and J. M. C. Plane (2009), First observation of micrometeoroid differential ablation in the atmosphere, *Geophys. Res. Lett.*, *36*, L06101, doi:10.1029/2009GL037389.

Kane, T. J., C. S. Gardner, Q. Zhou, J. D. Mathews, and C. A. Tepley (1993), Lidar, radar and airglow observations of a prominent sporadic Na/sporadic E layer event at Arecibo during AIDA-89, *J. Atmos. Sol. Terr. Phys.*, *55*, 499–511, doi:10.1016/0021-9169(93)90084-C.

Kelley, M. C. (1989), *The Earth's Ionosphere*, Academic, San Diego, Calif.

Maeda, S., S. Nozawa, Y. Ogawa, and H. Fujiwara (2005), Comparative study of the high-latitude E region ion and neutral temperatures in the polar cap and the auroral region derived from the EISCAT radar observations, *J. Geophys. Res.*, *110*, A08301, doi:10.1029/2004JA010893.

Mathews, J. D., Y. T. Morton, and Q. Zhou (1993), Observations of ion layer motions during the AIDA campaign, *J. Atmos. Terr. Phys.*, *55*, 447–457, doi:10.1016/0021-9169(93)90080-I.

Plane, J. M. C. (2003), Atmospheric chemistry of meteoric metals, *Chem. Rev.*, *103*, 4963–4984, doi:10.1021/cr0205309.

Plane, J. M. C., D. E. Self, T. Vondrak, and K. R. I. Woodcock (2003), Laboratory studies and modeling of mesospheric iron chemistry, *Adv. Space Res.*, *32*, 699–708, doi:10.1016/S0273-1177(03)00401-0.

Richmond, A. (1978), Gravity wave generation, propagation, and dissipation in the thermosphere, *J. Geophys. Res.*, *83*, 4131–4145, doi:10.1029/JA083iA09p04131.

Thayer, J. P., and J. Semeter (2004), The convergence of magnetospheric energy flux in the polar atmosphere, *J. Atmos. Sol. Terr. Phys.*, *66*, 807–824, doi:10.1016/j.jastp.2004.01.035.

Thome, G. D. (1964), Incoherent Scatter observations of traveling ionospheric disturbances, *J. Geophys. Res.*, *69*, 4047–4049, doi:10.1029/JZ069i019p04047.

Vadas, S. L. (2007), Horizontal and vertical propagation and dissipation of gravity waves in the thermosphere from lower atmospheric and thermospheric sources, *J. Geophys. Res.*, *112*, A06305, doi:10.1029/2006JA011845.

Vadas, S. L., and M. J. Nicolls (2009), Temporal evolution of neutral, thermospheric winds and plasma response using PFISR measurements of gravity waves, *J. Atmos. Sol. Terr. Phys.*, *71*, 744–770, doi:10.1016/j.jastp.2009.01.011.

Viereck, R. A., et al. (1996), $Mg^+$ and other metallic emissions observed in the thermosphere, *Adv. Space Res.*, *18*(3), 61–64, doi:10.1016/0273-1177(95)00839-7.

Vondrak, T., J. M. C. Plane, S. Broadley, and D. Janches (2008), A chemical model of meteoric ablation, *Atmos. Chem. Phys.*, *8*, 7015–7031, doi:10.5194/acp-8-7015-2008.

Zhou, Q. H., S. Raizada, C. A. Tepley, and J. M. C. Plane (2008), Seasonal and diurnal variation of electron and iron concentrations at the meteor heights above Arecibo, *J. Atmos. Sol. Terr. Phys.*, *70*, 49–60, doi:10.1016/j.jastp.2007.09.012.

C. Chen, X. Chu, W. Fong, and Z. Yu, Cooperative Institute for Research in Environmental Sciences and Department of Aerospace Engineering Sciences, University of Colorado at Boulder, 216 UCB, Boulder, CO 80309-0216, USA. (xinzhao.chu@colorado.edu)

C. S. Gardner, Department of Electrical and Computer Engineering, University of Illinois at Urbana-Champaign, 1406 W. Green St., Urbana, IL 61801-2918, USA.